J Mater Sci: Mater Electron (2013) 24:1758–1763
DOI 10.1007/s10854-012-1008-y

# Preparation of $TiO_2$ thick film by laser chemical vapor deposition method

**Dongyun Guo · Akihiko Ito · Takashi Goto · Rong Tu · Chuanbin Wang · Qiang Shen · Lianmeng Zhang**

Received: 22 September 2012 / Accepted: 17 November 2012 / Published online: 24 November 2012
© Springer Science+Business Media New York 2012

**Abstract** A $TiO_2$ film was prepared on Pt/Ti/$SiO_2$/Si substrate by a laser chemical vapor deposition method. The rutile $TiO_2$ film with pyramidal grains and columnar cross-section was obtained at a high deposition rate ($R_{dep}$ = 11.4 μm $h^{-1}$). At 300 K and 1 MHz, the dielectric constant ($\varepsilon_r$) and loss (tan$\delta$) of the $TiO_2$ film were about 73.0 and 0.0069, respectively. The electrical properties of $TiO_2$ film were investigated by ac impedance spectroscopy over ranges of temperature (300–873 K) and frequency ($10^2$–$10^7$ Hz). The Cole–Cole plots between real and imaginary parts of the impedance ($Z'$ and $Z''$) in the above frequency and temperature range suggested the presence of two relaxation regimes that were attributed to grain and grain boundary responses. The ionic conduction in the rutile $TiO_2$ film was dominated by the oxygen vacancies.

## 1 Introduction

The rutile $TiO_2$ films are widely investigated because they have many applications such as capacitor, sensors, antireflection coatings and corrosion-resistant barriers [1–5]. The dielectric constant ($\varepsilon_r$) of rutile $TiO_2$ crystal is anisotropic and has values of 170 in the *c* direction and 89 perpendicular to the *c* direction, which indicates that $TiO_2$ film has the possibility application to future ultra-large-scale dynamic random access memory (DRAM) [6, 7]. $TiO_2$ films have been prepared by many methods, such as sputtering, conventional chemical vapor deposition, sol–gel method, type-casting and laser chemical vapor deposition (LCVD) [8–15]. Among these methods, the high-quality film were prepared by LCVD with high deposition rate ($R_{dep}$). Goto et al. [15] prepared $TiO_2$ films on alumina plates with a mixture phase of rutile and anatase by LCVD with very high $R_{dep}$ (about 3,000 μm $h^{-1}$). Recently, Gao et al. [16] reported that the rutile $TiO_2$ films were deposited on Yttria-stabilized zirconia (YSZ) plates by LCVD, and the $R_{dep}$ was about 240 μm $h^{-1}$. However, they didn't study the dielectric property of the $TiO_2$ films. Numerous research indicated that the dielectric and electrical properties of $TiO_2$ films were dependent on their microstructure [17, 18]. The films prepared by LCVD always had the characteristic columnar cross-section [19–23]. It is necessary to investigate the electrical properties of the rutile $TiO_2$ film prepared by LCVD.

To investigate the dielectric property and electrical conductivity of the rutile $TiO_2$ film, a Pt/Ti/$SiO_2$/Si substrate, which had good electrical conductivity and thermal stability, was used to replace the ceramic substrates in references [15] and [16]. In this study, $TiO_2$ film was prepared on Pt/Ti/$SiO_2$/Si substrate by LCVD, and the dielectric properties and electrical conductivity of $TiO_2$ film were investigated.

## 2 Experimental

The $TiO_2$ film was prepared on Pt/Ti/$SiO_2$/Si substrates by LCVD with a continuous-wave Nd:YAG laser (wavelength: 1,064 nm). A schematic of the LCVD apparatus has

D. Guo (✉) · C. Wang · Q. Shen · L. Zhang
State Key Laboratory of Advanced Technology for Materials Synthesis and Processing, School of Materials Science and Engineering, Wuhan University of Technology, Wuhan 430070, China
e-mail: guodongyun@gmail.com

D. Guo · A. Ito · T. Goto · R. Tu
Institute for Materials Research, Tohoku University, Sendai 980-8577, Japan

**Table 1** Deposition conditions of $TiO_2$ film by LCVD

| | |
|---|---|
| Ti(Oi–Pr)$_2$ (dpm)$_2$ evaporation temperature ($T_{Ti}$) | 423 K |
| Substrate pre-heating temperature ($T_{pre}$) | 773 K |
| Total chamber pressure ($P_{tot}$) | 600 Pa |
| Gas flow rate | |
| Ar gas ($FR_{Ar}$) | $8.3 \times 10^{-7}$ m$^3$ s$^{-1}$ |
| $O_2$ gas ($FR_{O2}$) | $1.7 \times 10^{-6}$ m$^3$ s$^{-1}$ |
| Laser power ($P_L$) | 48 W |
| Deposition time ($t$) | 1,800 s |
| Substrate-nozzle distance | 30 mm |
| Substrate | Pt/Ti/SiO$_2$/Si ($10 \times 10 \times 0.5$ mm$^3$) |

been reported elsewhere [19, 20]. The substrate was put on a hot stage with a pre-heating temperature ($T_{pre}$) of 773 K. A thermocouple was inserted at the bottom side of the substrate to measure the deposition temperature ($T_{dep}$). In this study, $T_{dep}$ was 858 K. A laser beam, 14 mm in diameter, was introduced through a quartz window to irradiate the whole substrate. The laser power ($P_L$) was 48 W. The titanium diisopropoxy-dipivaloylmethanate (Ti(Oi–Pr)$_2$ (DPM)$_2$, Toshima Manufactory) precursor was heated at 423 K, and the vapor was carried into the chamber with Ar gas. The $O_2$ gas was separately introduced into the chamber through a double-tube gas nozzle. The total pressure ($P_{tot}$) in the CVD chamber was held at 600 Pa. The deposition was conducted for 1,800 s. Details of the deposition conditions are listed in Table 1.

The crystal structure was analyzed by X-ray diffraction (XRD, Rigaku RAD—2C) using CuKα X-ray radiation. The surface and cross section microstructures were observed by a scanning electron microscope (SEM, Hitachi S-3100H). To measure the impedance spectroscopy, the top electrode was fabricated on the surface of the $TiO_2$ film from Au paste, which was dried and decomposed by gradually heating to 1,073 K. Impedance spectroscopic measurements were performed using an impedance/grain-phase analyzer (Hewlett Packard 4194) at an ac driving voltage of 10 mV in the temperature range from 300 to 873 K over the frequency range of $10^2$–$10^7$ Hz.

## 3 Results and discussions

Figure 1 shows the XRD pattern of $TiO_2$ film. It was indexed to the rutile $TiO_2$ phase (JCPDS 21-1276). The single-phase $TiO_2$ film was obtained. Figure 2 displays the cross-sectional and surface SEM images. As shown in Fig. 2a, the $TiO_2$ film had columnar cross-section, and the film thickness was about 5.7 μm that indicated the $R_{dep}$ was 11.4 μm h$^{-1}$, which was slower than these reported by

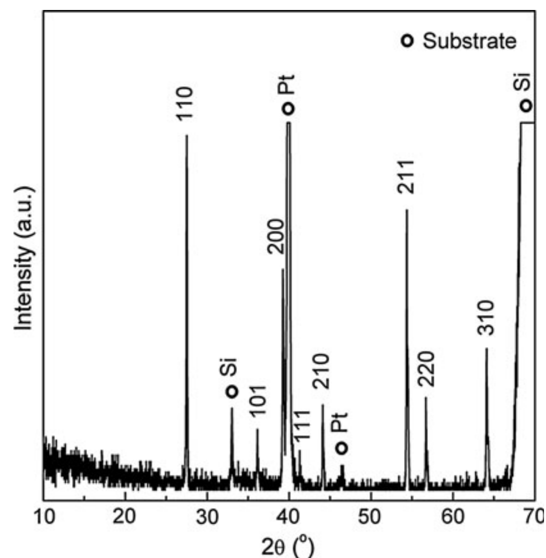


**Fig. 1** XRD pattern of the $TiO_2$ film

Goto et al. [15] and Gao et al. [16] due to the low $T_{Ti}$ in this study. However, the present $R_{dep}$ was still much higher than that prepared by other methods [8–13]. The surface consisted of pyramidal grains. Figure 2c shows the schematic of crystal structure, which was illustrated by VESAT, a three-dimensional visualization system [24]. In the rutile crystal structure, the basic building block consists of a titanium atom surrounded by six oxygen atoms in a more or less distorted $TiO_6$ octahedral configuration. The two bonds between the titanium and the oxygen atoms at the apices of the octahedron are slightly longer [1]. The pyramidal grains in the surface of $TiO_2$ film, as shown in Fig. 2b, were attributed to the stacked $TiO_6$ octahedral.

Figure 3 presents the temperature dependence of dielectric properties of the $TiO_2$ film in the temperature range from 300 to 873 K at 1 MHz. At 300 K, the $\varepsilon_r$ and dielectric loss (tan$\delta$) of the $TiO_2$ film were about 73.0 and 0.0069, respectively. The $\varepsilon_r$ value in this work was close to those of the rutile $TiO_2$ crystal perpendicular to the $c$ direction and the rutile $TiO_2$ film prepared by Kim et al. [6, 7] which also indicated the single-phase rutile $TiO_2$ film was prepared by LCVD. With increasing temperature, the $\varepsilon_r$ slightly decreased, and then increased. A peak around 753 K was observed, which indicated that there was a phase transition. Generally, the transition temperature is about 1,173 K. However, it also depends on pressure, stress, contaminants, oxygen deficiency, etc. [25]. The tan$\delta$ increased slightly with increasing temperature from 300 to 753 K. As temperature was beyond 753 K, the tan$\delta$ abruptly increased due to the phase transition.

Figure 4 depicts the frequency dependence of the imaginary part of impedance ($Z''$) at different temperatures. At 300 K, there was no peak in the measured frequency range,

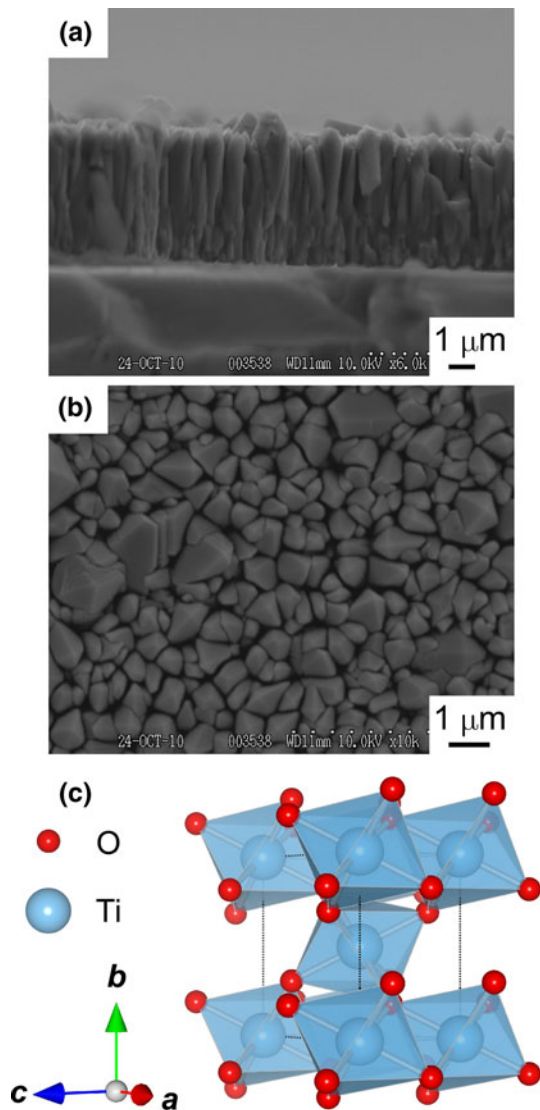


**Fig. 2** Cross section **a** and surface **b** microstructures of the $TiO_2$ film, and ball-and-stick model of the rutile $TiO_2$ crystal structure **c**

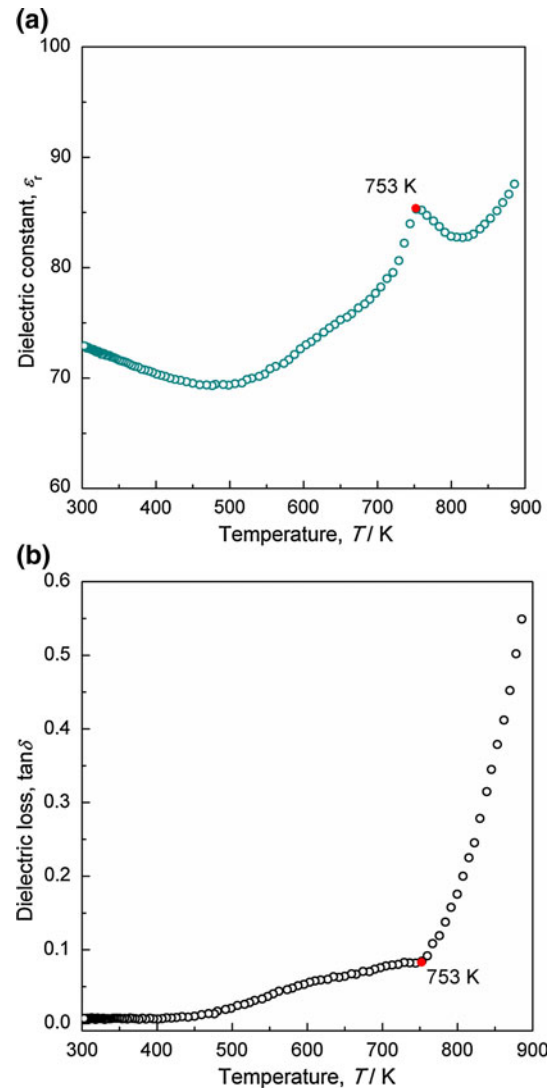


**Fig. 3** Temperature dependence of dielectric properties for the $TiO_2$ film: **a** dielectric constant ($\varepsilon_r$) and **b** dielectric loss ($\tan\delta$)

since the film had high resistance. With increasing the temperature, the resistance decreased and the peaks ($Z''_{max}$) with characteristic frequency maximum ($f_{max}$) were observed due to the grain effect. The peaks were suggestive of relaxation processes with a spread of relaxation time, which were temperature dependent. As temperature increased, the $f_{max}$ shifted to higher frequency and the $Z''_{max}$ decreased due to the decrease of resistance of $TiO_2$ film.

Figure 5a depicts the Cole–Cole plots of complex impedance data (the imaginary part $Z''$ and the real part $Z'$) at different temperatures. The arrows in Fig. 5a showed the direction of increasing frequency. At low temperatures, an almost straight line with big slope was observed due to high resistance. With increasing temperature, the resistance decreased and the impedance semicircles were observed. Figure 5b shows the enlarged Cole–Cole plot obtained at 870 K. There were two semicircles, which suggested the presence of two relaxations that were attributed to grain and grain-boundary responses. To analyze and interpret the Cole–Cole plots, an equivalent circuit model comprising two parallel *RC* elements in series was established as shown in Fig. 5c. The low-frequency semicircle corresponded to the grain-boundary response ($R_{gb}C_{gb}$) and the high-frequency one corresponded to the grain response ($R_gC_g$). Figure 5b showed the good agreement between the experimental data (triangular patterns) and the theoretical curve (dotted line, generated from ZVIEW software).

Figure 6 shows the ac electrical conductivity plots as a function of frequency at different temperatures. At 562 K, the conductivity–frequency curve had a frequency-independent dc component at low frequency (100–$10^4$ Hz) and

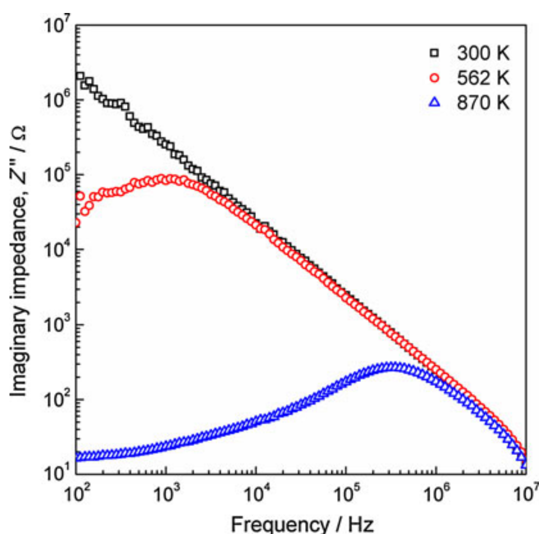


**Fig. 4** Imaginary impedance ($Z''$) as a function of frequency for the $TiO_2$ film

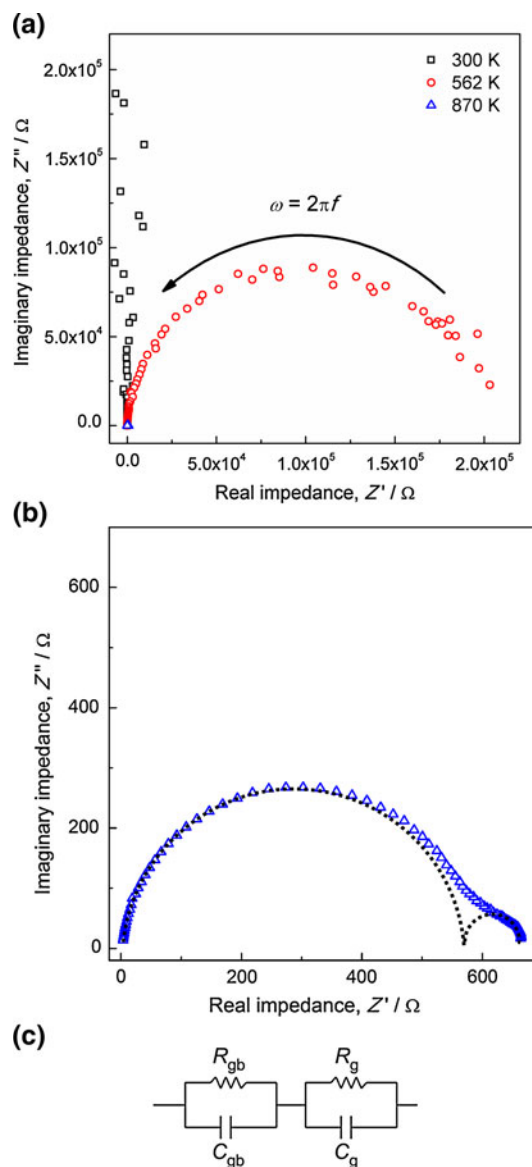


**Fig. 5** Complex impedance plots ($Z'$ vs $Z''$) of the $TiO_2$ film: **a** at different temperatures **b** the enlarged impedance plot of data obtained at 870 K, and **c** equivalent circuit used to represent the electrical properties of the grain and grain-boundary effects

a frequency-dependent ac component at high frequency ($10^4$–$10^7$ Hz). With increasing temperature, the curves tended to flatten. Salam et al. [26] analyzed the frequency dependent ac electrical conductivity data and proposed the frequency dependence of electrical conductivity to be of the form

$$\sigma(\omega) = \sigma(0) + A_1\omega^{n1} + A_2\omega^{n2} \quad (1)$$

where $\sigma(\omega)$ is the total conductivity, $\sigma(0)$ is the frequency-independent conductivity, and the coefficient $A$ and exponent $n$ are temperature and material dependent. The frequency-independent plateau at the low frequency was associated with the term $\sigma(0)$ contributing to dc conductivity. As frequency increased, two dispersion regions appeared for all temperatures. The mid-frequency dispersion ($A_1\omega^{n1}$) was associated with the grain boundaries, while the high-frequency one ($A_2\omega^{n2}$) with the grains [27, 28]. The electrical conductivity of grain ($\sigma_g$) was obtained from the grain resistance ($R_g$) using the relation.

$$\sigma_g = \frac{t}{R_g A} \quad (2)$$

where $t$ is the film thickness and $A$ is the electrode area. The temperature dependence of $\sigma_g$ in Arrhenius format was described by

$$\sigma_g = \sigma_0 \exp(-E_a/kT) \quad (3)$$

where $\sigma_0$ is the pre-exponential factor, $E_a$ the activation energy for the conduction process, $k$ the Boltzmann constant and $T$ the absolute temperature. The Arrhenius plot of $\sigma_g$ is shown in Fig. 7. The values of $E_a$ for the grain conduction at high-temperature region (744–873 K) and low-temperature region (555–744 K) were 1.06 and 0.69 eV, respectively. This result indicated that the different conductive mechanisms dominated in the different temperature regions. $TiO_2$ can be hardly oxidized but easily reduced to $TiO_{2-x}$ contains extra Ti and/or missing O atoms, which suggests that the dominant native point defects should be the oxygen vacancy $V_O$ and the titanium interstitial $Ti_I$ [29]. Iddir et al. [30] calculated the diffusion barriers of $V_O^{2+}$ defect. They investigated the diffusion of $V_O^{2+}$ by moving the oxygen vacancy along three paths (path A along [001], B along [$1\bar{1}0$] and C from the plane to the apex position of the octahedron) in the $TiO_6$ octahedron.

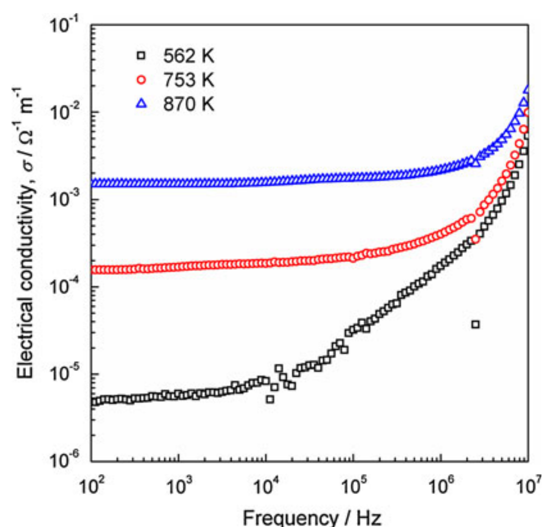


**Fig. 6** Frequency dependence plots of the ac electrical conductivity of the $TiO_2$ film at different temperatures

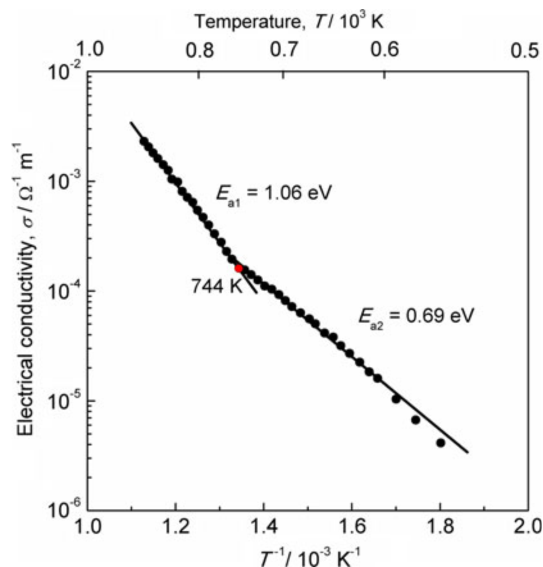


**Fig. 7** Temperature dependence of the grain conductance for the $TiO_2$ film

The diffusion barriers along path A, B and C were 1.77, 0.69 and 1.10 eV, respectively. According to Fig. 2b, the columnar cross-section consisted of the stacked $TiO_6$ octahedral. The $E_a$ of 0.69 eV indicated that the migration of oxygen vacancy along path B dominated at the temperature range of 555–744 K. As the temperature was near 744 K, the phase transition happened. And at the temperature range of 744–873 K, the $E_a$ of 1.06 eV was close to the 1.10 eV, which indicated that the migration of oxygen vacancy along path C dominated. In the present study, the ionic conduction in the rutile $TiO_2$ film was dominated by the oxygen vacancies.

## 4 Conclusions

The rutile $TiO_2$ film was prepared on Pt/Ti/$SiO_2$/Si substrate with high $R_{dep}$ (11.4 μm $h^{-1}$) by LCVD. The $TiO_2$ film consisted of pyramidal grains with columnar cross-section. At 300 K and 1 MHz, the $\varepsilon_r$ and tan$\delta$ of the $TiO_2$ film were about 73.0 and 0.0069, respectively. The $E_a$ of the grain conduction in the $TiO_2$ film at high-temperature region (744–873 K) and low-temperature region (555–744 K) were 1.06 and 0.69 eV, respectively. The ionic conduction in the rutile $TiO_2$ film was dominated by the oxygen vacancies. At 555–744 K, the migration of oxygen vacancy along path B dominated at the temperature range. And the migration of oxygen vacancy along path C dominated at 744–873 K.

**Acknowledgments** This work was supported in part by Global COE Program of the Materials Integration, Tohoku University, and by the International Science and Technology Cooperation Program of China (Grant No. 2009DFB50470).

## References

1. U. Diebold, Surf. Sci. Rep. **48**, 53–229 (2003)
2. M. Kadoshima, M. Hiratani, Y. Shimamoto, K. Torii, H. Miki, S. Kimura, T. Nabatame, Thin Solid Films **424**, 224–228 (2003)
3. D.A.H. Hanaor, C.C. Sorrell, J. Mater. Sci. **46**, 855–874 (2011)
4. A. Fujishima, X. Zhang, D.A. Tryk, Surf. Sci. Rep. **63**, 515–582 (2008)
5. A. Fujishima, K. Honda, Nature **238**, 37–38 (1972)
6. R.A. Parker, Phys. Rev. **124**, 1719–1722 (1961)
7. S.K. Kim, W. Kim, K. Kim, C. Hwang, J. Jeong, Appl. Phys. Lett. **85**, 4112–4114 (2004)
8. P. Alexandrov, J. Koprinarova, D. Todorov, Vacuum **47**, 1333–1336 (1996)
9. N. Rausch, E.P. Burte, J. Electrochem. Soc. **140**, 145–149 (1993)
10. Q. Zhang, G.L. Griffin, Thin Solid Films **263**, 65–71 (1995)
11. J.Y. Kim, H.S. Jung, J.H. No, J.R. Kim, K.S. Hong, J. Electroceram. **16**, 447–451 (2006)
12. I. Oja, A. Mere, M. Krunks, R. Nisumaa, C.H. Solterbeck, M. Es-Souni, Thin Solid Films **515**, 674–677 (2006)
13. C. Sheng, D. Fatih, Int. J. Appl. Ceram. Technol. **8**, 1363–1373 (2011)
14. M. Gao, A. Ito, R. Tu, T. Goto, Key Eng. Mater. **508**, 287–290 (2012)
15. T. Goto, T. Kimura, Key Eng. Mater. **317–318**, 495–500 (2006)
16. M. Gao, A. Ito, R. Tu, T. Goto, Key Eng. Mater. **508**, 279–282 (2012)
17. C. Demetry, X. Shi, Solid State Ionics **118**, 271–279 (1999)
18. C. Sheng, P. Vladimir, D. Fatih, J. Am. Ceram. Soc. **93**, 3031–3034 (2010)
19. D. Guo, T. Goto, C. Wang, Q. Shen, L. Zhang, J. Mater. Sci.: Mater. Electron. **23**, 897–900 (2012)
20. D. Guo, T. Goto, C. Wang, Q. Shen, L. Zhang, Mater. Lett. **70**, 135–137 (2012)
21. D. Guo, A. Ito, T. Goto, R. Tu, C. Wang, Q. Shen, L. Zhang, J. Mater. Sci. **47**, 1559–1561 (2012)
22. D. Guo, T. Goto, C. Wang, Q. Shen, L. Zhang, Appl. Surf. Sci. **258**, 7860–7863 (2012)

23. D. Guo, T. Goto, C. Wang, Q. Shen, L. Zhang, J. Electron. Mater. **41**, 689–694 (2012)
24. K. Momma, F. Izumi, J. Appl. Crystallogr. **41**, 653–658 (2008)
25. J.M. Criado, C. Real, J. Soria, Solid State Ionics **32–33**, 461–465 (1989)
26. F. Salam, J.C. Giuntini, S.S. Soulayman, J.V. Zanchetta, Appl. Phys. A **63**, 447–452 (1996)
27. A. Pelaiz-Barranco, M.P. Gutierrez-Amador, A. Huanosta, R. Valenzuela, Appl. Phys. Lett. **73**, 2039–2041 (1998)
28. N. Ortega, A. Kumar, P. Bhattacharya, S.B. Majumder, R.S. Katiyar, Phys. Rev. B **77**, 014111 (2008)
29. A.M. Asaduzzaman, P. Kruger, J. Phys. Chem. C **114**, 19649–19652 (2010)
30. H. Iddir, S. Ogut, P. Zapol, N.D. Browning, Phys. Rev. B **75**, 073203 (2007)